

# An LTCC Coupled Resonator Decoupling Network for Two Antennas

Kewei Qian, Luyi Zhao, *Member, IEEE*, and Ke-Li Wu, *Fellow, IEEE*

**Abstract**—An integrated low-temperature co-fired ceramic (LTCC) coupled resonator decoupling network (CRDN) for two coupled antennas is proposed in this paper. By virtue of LTCC technology, a second-order CRDN is realized by two tightly coupled lumped-element resonators in a volume of  $3.2 \times 2.5 \times 1.2 \text{ mm}^3$ . Theoretical analysis has revealed that a wide range of mutual admittance of a CRDN can be realized by choosing appropriate I/O coupling elements while the coupled resonators can be consolidated in an LTCC device. This “one-fit-all” feature allows for decoupling a wide range of coupled antennas with different form factors for a given frequency band. To prove the concept, two LTCC CRDNs for decoupling different forms of antennas working in the 2.45-GHz band are designed, fabricated, and tested. Measurement results have demonstrated that significant improvement in isolation can be achieved within a wide operating frequency range in all cases. The presented design theory and circuit topology are general and can be applied to both symmetric and asymmetric two-element antenna arrays.

**Index Terms**—Coupled resonator decoupling network (CRDN), low-temperature co-fired ceramic (LTCC), multiple-input multiple-output (MIMO) antenna array.

## I. INTRODUCTION

TO SATISFY the fast growing demands from the mobile internet market for higher data rate and better quality of service (QoS) on wireless communication systems, many advanced technologies for increasing the data throughput have been put into use. Among them, the multiple input multiple output (MIMO) data accessing scheme, a proven technology to effectively use the multipath environment, has been becoming a compulsory option in today’s wireless communication systems in both base stations and mobile terminals. With the MIMO technology, digital transceivers are used to combine the data

streams arriving at multiple antennas, which are assumed to be uncorrelated when the mutual couplings among the antennas are ideally zero. Along with orthogonal frequency division multiplex (OFDM), spatial multiplexing, diversity coding, and other signal-processing techniques, a MIMO system can largely improve data throughput and system performance [1], [2].

However, due to inevitable strong mutual couplings between antennas in a wireless terminal, such as a fourth-generation (4G) long-term evolution (LTE) smart phone, the mutual coupling and spatial correlation between antennas become severe, which diminishes the channel capacity gain of a MIMO system due to a strong signal correlation. Additionally, a strong coupling also lowers the radiation efficiency as the coupled antenna becomes a resistive load of the transmitting antenna. All of these negative effects decrease the superiority of a MIMO system and deteriorate the system performance. Therefore, tremendous research efforts have been devoted to reducing the mutual couplings among MIMO antennas in recent years [3].

Recently, some typical antenna configurations and locations in a terminal are studied to illustrate the effect of characteristic mode and current localization on the isolation level between antenna elements [4]. It has been shown that by properly exciting the characteristic mode and the chassis current, angle diversity as well as polarization diversity can be achieved. For symmetric arrays, an eigendecomposition network can be designed for inherently decoupling a coupled antenna array by decomposing the input signals into two or more orthogonal eigenmodes of the array [5]–[7].

A simple decoupling network, which consists of two transmission lines and a shunt reactive element, is proposed for reducing the coupling of two strongly coupled antennas [8]. Good isolation can be achieved in a compact size. A practical concern for this scheme is its relative narrow decoupling bandwidth (about 3% for 20-dB isolation) due to the fact that the mutual admittance of a shunt reactive element is not stationary within the band of interest. Moreover, since the zero of self-admittance locates either at  $\omega = 0$  or  $\omega = \infty$ , which is far away from the resonant frequency of the antennas, two additional matching networks are required for impedance matching. A neutralization line [9]–[11] and parasitic scattering [12] techniques are effective methods to reduce mutual couplings between the antennas for narrow bandwidth applications. By reproducing an opposite coupling to the unwanted one, less mutual coupling at certain frequencies can be obtained. Planar electromagnetic-bandgap (EBG) structures [13]–[15] and defected ground structures (DGSs) [16], [17], which act as bandstop filters for surface waves, are also proposed to realize certain level of isolation between antennas.

Manuscript received April 14, 2015; revised June 12, 2015; accepted July 27, 2015. Date of publication August 18, 2015; date of current version October 02, 2015. This work was supported by The Chinese University of Hong Kong under a Postgraduate Scholarship. This work was supported in part by the Development and Reform Commission of Shenzhen Municipality under Grant Shen Fa Gai (2013)1673.

K. Qian was with the Department of Electronic Engineering and the Engineering Laboratory of Wireless Locating Technology and System, Shenzhen Research Institute, The Chinese University of Hong Kong, Shatin, NT, Hong Kong. He is now with the Electronic Science Research Institute, University of Electronic Science and Technology of China, Chengdu 610051, China (e-mail: kwqian@ee.cuhk.edu.hk).

L. Zhao and K.-L. Wu are with the Department of Electronic Engineering and the Engineering Laboratory of Wireless Locating Technology and System, Shenzhen Research Institute, The Chinese University of Hong Kong, Shatin, NT, Hong Kong (e-mail: lyzhao@ee.cuhk.edu.hk; klwu@ee.cuhk.edu.hk).

Color versions of one or more of the figures in this paper are available online at <http://ieeexplore.ieee.org>.

Digital Object Identifier 10.1109/TMTT.2015.2464816

Most recently, a new technique named the coupled resonator decoupling network (CRDN) is proposed for decoupling two and three strongly coupled antennas [18]–[21]. The basic underlying principle is to design a second-order or higher order coupled resonator network that is connected to the two coupled antennas in shunt and is with the mutual admittance opposite to that of the two coupled antennas such that the unwanted mutual coupling of the antennas can be canceled in a relatively wide frequency band.

Three major issues concerning the above existing decoupling techniques are as follows:

- 1) the realization of these decoupling schemes is antenna and its periphery specific;
- 2) the bandwidth and the required space are mutually exclusive; a wideband solution usually requires an impractically large real estate;
- 3) more importantly, there is no integrated solution that enables a miniaturized passive device to be used on high-density circuit boards of mobile terminals.

In order to achieve good isolation between two strongly coupled antennas in a mobile terminal, a small footprint and surface mountable device that is independent to the form factors of the antennas would be highly desirable. In this paper, an integrated CRDN for two strongly coupled antennas of arbitrary form factors is proposed. The CRDN is composed of two parts: a two-port multilayered LTCC device that consists of two tightly coupled lumped-element resonators, and an  $L$  or  $C$  component along with a transmission line external to each port of the LTCC device for customized I/O couplings. This circuit configuration allows one LTCC CRDN device for different antenna couplings of various antenna form factors. Furthermore, it will be shown that a tradeoff between the isolation level and decoupling bandwidth for a given operating frequency band can also be achieved. Therefore, with one consolidated LTCC device, which is designed for a given frequency band, and specific I/O coupling circuits external to the device, the proposed integrated CRDN is a “one-fit-all” solution for simultaneous decoupling and matching of various coupled antennas.

Although the original concept of the CRDN was proposed in [18]–[21], this paper attempts, for the first time, the following:

- 1) to develop the theory for designing an integrated lumped-element CRDN;
- 2) to demonstrate the feasibility and superiority of an integrated CRDN device;
- 3) to theoretically prove and experimentally justify the “one-fit-all” concept of the CRDN technology.

This paper has no intention to discuss how to design an LTCC lumped-element device, as it has been very well covered in the literature [22], [23].

This paper is organized as follows. Section II presents the theory for designing a lumped-element CRDN that simultaneously meets the decoupling and matching conditions. The dependence of the inter-resonator coupling on the decoupling bandwidth and the decoupling level is discussed. Section III gives four design examples of the LTCC CRDN scheme; two for symmetric arrays and two for asymmetric arrays, all of which use the same LTCC CRDN device. Good agreement between the electromagnetic (EM) designed

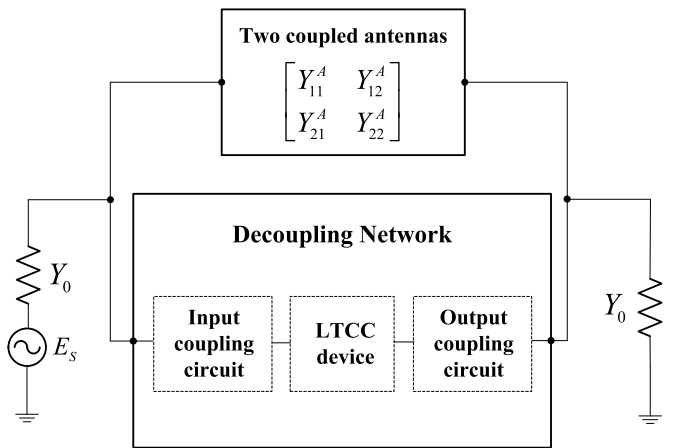


Fig. 1. Network representation of two coupled antennas in shunt with an LTCC CRDN circuit.

and measured results demonstrates the feasibility of this “one-fit-all” integrated solution. Additionally, a tradeoff analysis between the decoupling bandwidth and level is elaborated in Section IV. The practical examples demonstrate that the proposed CRDN technique is very suitable for different circumstances of mobile terminals. Finally, conclusions are given in Section V.

## II. DESIGN THEORY

### A. Decoupling and Matching Conditions

In the following discussion, two coupled antennas are represented by a  $2 \times 2$  admittance matrix defined in terms of the total voltages and currents at the two antenna ports. An LTCC CRDN circuit that consists of a consolidated LTCC chip and two I/O coupling elements is connected in shunt to the coupled antennas, as shown in Fig. 1. The admittance of the connected network is the sum of the two individual admittance matrices, i.e.,

$$Y = \begin{bmatrix} Y_{11} & Y_{12} \\ Y_{21} & Y_{22} \end{bmatrix} = \begin{bmatrix} Y_{11}^A + Y_{11}^N & Y_{12}^A + Y_{12}^N \\ Y_{21}^A + Y_{21}^N & Y_{22}^A + Y_{22}^N \end{bmatrix} \quad (1)$$

where  $Y^A$  and  $Y^N$  represent the admittance matrices of the coupled antennas and the decoupling network, respectively.

Obviously, good isolation between the two ports of the connected network can be achieved in the vicinity of the resonant frequency of the coupled antennas if

$$Y_{21}(\omega_r) = Y_{21}^A(\omega_r) + Y_{21}^N(\omega_r) \approx 0 \quad (2)$$

where  $\omega_r$  is the resonant angular frequency of the antennas.

Since the designed decoupling network is assumed to be lossless, the entries of the admittance matrix  $Y^N$  are purely imaginary. However, the admittance matrix  $Y^A$  for the antennas is complex in general. Thus, the decoupling condition can be simplified as

$$\text{Re} \{ Y_{21}^A(\omega_r) \} \approx 0 \quad (3a)$$

$$\text{Im} \{ Y_{21}^A(\omega_r) \} + \text{Im} \{ Y_{21}^N(\omega_r) \} \approx 0. \quad (3b)$$

Assuming that the coupled antennas are well matched at the resonant frequency, i.e.,  $Y_{11}^A(\omega_r) = Y_{22}^A(\omega_r) \approx Y_0$ , (3a) can

be realized at  $\omega_r$  by introducing a piece of transmission line of electrical length  $\theta_L$  and characteristic impedance  $Z_0$  at each antenna port. Supposing the coupling coefficient of the original antenna array is expressed as  $|S_{21}|e^{j\phi_{21}}$  in general,  $\theta_L$  can be chosen such that [8]

$$\theta_L = \frac{1}{2} \left[ \phi_{21} \pm \left( k\pi - \frac{\pi}{2} \right) \right], \quad k = 1, 2, 3L. \quad (4)$$

Similarly, when the decoupling condition is satisfied, which means  $S_{21} = 0$ , the matching condition can be expressed as

$$\text{Re} \{ Y_{ii}^A(\omega_r) \} \approx Y_0, \quad i = 1, 2 \quad (5a)$$

$$\text{Im} \{ Y_{ii}^A(\omega_r) \} + \text{Im} \{ Y_{ii}^N(\omega_r) \} \approx 0, \quad i = 1, 2. \quad (5b)$$

Since the antennas are assumed to be matched at  $\omega_r$ , (5b) can be simplified to

$$\text{Im} \{ Y_{ii}^N(\omega_r) \} \approx 0, \quad i = 1, 2. \quad (6)$$

### B. Design Equations and Procedure

A schematic circuit of the decoupling network is depicted in Fig. 2, where a well-known second-order coupled resonator filter topology is adopted. For simplicity, it is assumed that  $Z_1 = Z_0 = 50 \Omega$ . Denoting the  $[ABCD]$  matrix of the LTCC device by  $[\overline{ABCD}]$ , whose entries can be expressed as

$$\overline{A} = \overline{D} = \frac{\omega^2 L_1 (C_1 + C_2) - 1}{\omega^2 L_1 C_2} \quad (7a)$$

$$\overline{B} = \frac{1}{j\omega C_2} \quad (7b)$$

$$\overline{C} = \frac{2}{j\omega L_1} + 2j\omega C_1 - \frac{1}{j\omega^3 L_1^2 C_2} - \frac{\omega C_1^2}{jC_2} + \frac{2C_1}{j\omega L_1 C_2}. \quad (7c)$$

The  $[ABCD]$  matrix of the LTCC device cascaded with the I/O coupling circuits is converted to an admittance matrix to satisfy the matching and decoupling conditions stipulated by (3) and (6). The resultant equations are given by (8a) and (8b), shown at the bottom of this page, where  $C_A$  is a constant that opposites to the imaginary part of the mutual admittance of the two coupled antennas at the resonant frequency.

According to (7) and (8), the decoupling and matching conditions are decided by variables  $L_1$ ,  $C_1$ ,  $C_2$ ,  $C_3$ , and  $\theta_1$ , which can be determined by the following procedure.

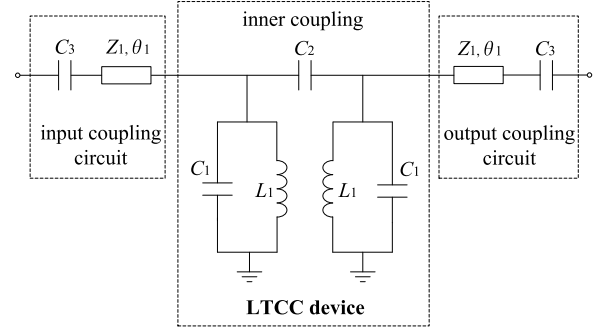


Fig. 2. Architecture of an integrated CRDN scheme.

- 1) The values of  $L_1$  and  $C_1$  of the LC tank are determined by the resonant frequency of the coupled antennas.
- 2) The mutual coupling capacitance  $C_2$  is designed to be as large as possible to realize a flat  $\text{Im}\{Y_{21}^N\}$  response in the operating band. In the following examples, this value is chosen to be 6 pF due to the LTCC fabrication constraints.
- 3) A unique solution for variables  $C_3$  and  $\theta_1$  can be found by solving simultaneous nonlinear equations (8a) and (8b).

For illustration purpose, the loci of the principal value of the two equations of  $\text{Im}\{Y_{21}^N\}$  from 0.008 to 0.019 are plotted in Fig. 3. It is shown that the stronger the mutual coupling is, the larger the capacitor  $C_3$  and the shorter the  $\theta_1$  are required. For example, when  $\text{Im}\{Y_{21}^N\} = 0.012$ , the intersection of the two sets of loci shows the solution of  $C_3 = 2.7$  pF and  $\theta_1 = 46^\circ$ .

It should be mentioned that parameter  $C_3$  is crucial and can be adjusted to accommodate different value of mutual coupling; and  $\theta_1$  can be used to compensate the frequency offset introduced by  $C_3$ .

### C. One-Fit-All Scheme

From (8a) and (8b), it is shown that admittance parameters of the decoupling network depend on the values of  $\theta_1$  and  $C_3$ , while the  $[\overline{ABCD}]$  matrix remains unchanged. In other words, different mutual admittances of a CRDN can be achieved by only changing I/O couplings when the LTCC device is consolidated for a given frequency band. For instance, the simulated imaginary part of  $Y_{21}^N$  with different  $C_3$  and  $\theta_1$  for I/O couplings are presented in Fig. 4. It can be seen that when  $L_1 = 1.5$  nH,  $C_1 = 0.7$  pF, and  $C_2 = 4.9$  pF are fixed, different levels of  $\text{Im}\{Y_{21}^N\}$  (from 0.008 to 0.019) can be obtained in a wideband

$$\text{Im} \left[ \frac{-1}{2j\overline{A} \left( \cos \theta_1 + \frac{\sin \theta_1}{Z_0 \omega C_3} \right) \cdot \left( Z_0 \sin \theta_1 - \frac{\cos \theta_1}{\omega C_3} \right) + \overline{B} \left( \cos \theta_1 + \frac{\sin \theta_1}{Z_0 \omega C_3} \right)^2 - \overline{C} \left( Z_0 \sin \theta_1 - \frac{\cos \theta_1}{\omega C_3} \right)^2} \right] = -\text{Im} [Y_{21}^A] = C_A \quad (8a)$$

$$\text{Im} \left[ \frac{\overline{A} \cdot \left[ \cos \theta_1 \cdot \left( \cos \theta_1 + \frac{\sin \theta_1}{Z_0 \omega C_3} \right) - \sin \theta_1 \cdot \left( \sin \theta_1 - \frac{\cos \theta_1}{Z_0 \omega C_3} \right) \right] + \frac{j\overline{B}}{Z_0} \sin \theta_1 \cdot \left( \cos \theta_1 + \frac{\sin \theta_1}{Z_0 \omega C_3} \right) + j\overline{C} \cos \theta_1 \left( Z_0 \sin \theta_1 - \frac{\cos \theta_1}{\omega C_3} \right)}{2j\overline{A} \left( \cos \theta_1 + \frac{\sin \theta_1}{Z_0 \omega C_3} \right) \cdot \left( Z_0 \sin \theta_1 - \frac{\cos \theta_1}{\omega C_3} \right) + \overline{B} \left( \cos \theta_1 + \frac{\sin \theta_1}{Z_0 \omega C_3} \right)^2 - \overline{C} \left( Z_0 \sin \theta_1 - \frac{\cos \theta_1}{\omega C_3} \right)^2} \right] = 0 \quad (8b)$$

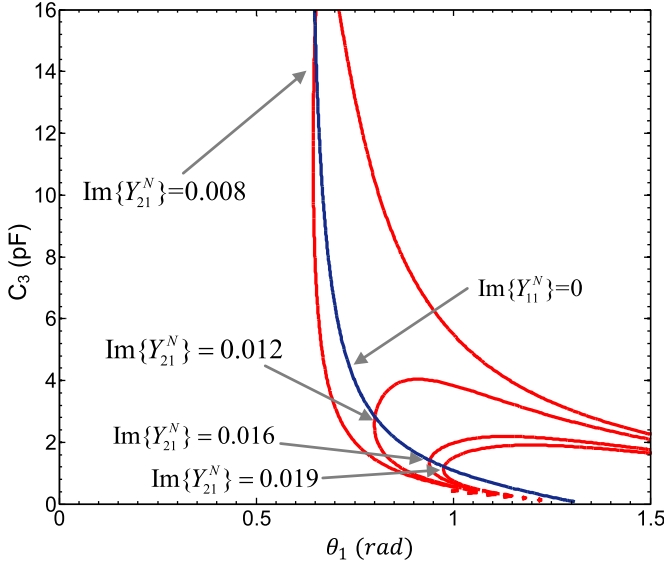


Fig. 3. Loci of the principal value of (8a) and (8b) for  $\text{Im}\{Y_{21}^N\} = 0.008$  to  $0.019$  (S) when  $L_1 = 1.5$  nH,  $C_1 = 0.7$  pF, and  $C_2 = 4.9$  pF.

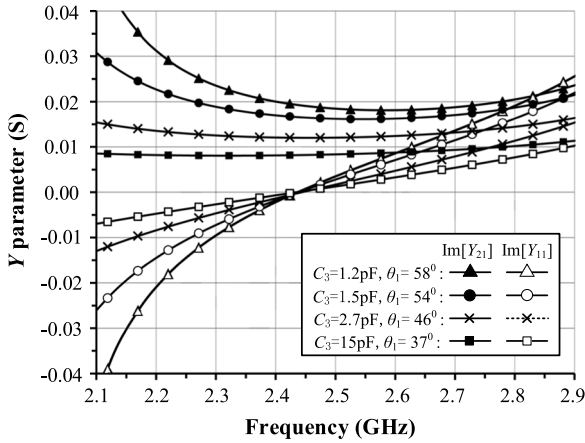


Fig. 4. Simulated  $Y$ -parameters of the decoupling network with different I/O coupling circuit values.

sense by only adjusting  $C_3$  and  $\theta_1$ , while  $\text{Im}\{Y_{11}^N\}$  remains to be zero at 2.44 GHz for good matching in all cases. It can be seen that the results in Fig. 4 match the solution shown in Fig. 3. This “one-fit-all” feature is very attractive because it allows of an antenna independent LTCC CRDN component for a wide range of antenna form factors. It should be pointed out that a  $45^\circ$  transmission line at  $\omega_r$  at each port of the CRDN for connecting purpose is omitted in Fig. 2.

Moreover, it should be mentioned that antennas with positive  $\text{Im}\{Y_{21}^A\}$  can also be decoupled by this network topology with corresponding negative  $\text{Im}\{Y_{21}^N\}$  realized by using an inductive inter-resonator coupling.

#### D. Decoupling Bandwidth Analysis

It can be observed that various types of practical coupled antennas, such as patches, monopoles, or planar inverted-F antennas (PIFAs),  $\text{Im}\{Y_{21}^A\}$  is almost a constant in the vicinity of the resonant frequency in most cases. According to (3), if a wide decoupling bandwidth is required,  $Y_{21}^N$  of the decoupling

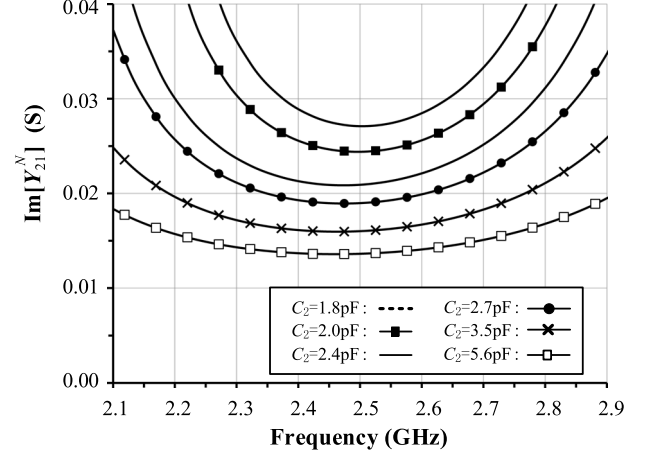


Fig. 5. Simulated results of  $\text{Im}\{Y_{21}^N\}$  for different  $C_2$  values.

network needs to be as constant as possible and be opposite to  $\text{Im}\{Y_{21}^A\}$  within the band of interest, that is to say

$$\begin{aligned} \text{Im}\{Y_{21}^N(\omega)\} |_{\omega \in [\omega_r - \Delta\omega, \omega_r + \Delta\omega]} &\approx \text{Im}\{Y_{21}^N(\omega_r)\} \\ &= -\text{Im}\{Y_{21}^A(\omega_r)\} \end{aligned} \quad (9)$$

where  $[\omega_r - \Delta\omega, \omega_r + \Delta\omega]$  is the frequency band of interest. In other words, the decoupling bandwidth, which is related to the slope of  $Y_{21}^N$  at  $\omega_r$ , becomes wider as the slope approaches zero. The previous research has shown that the coupling between the two resonators has a direct impact on the slope of  $Y_{21}^N$  at the resonant frequency [20]. In this paper, a capacitive mutual coupling is utilized. As illustrated in Fig. 5,  $\text{Im}\{Y_{21}^N\}$  can be approximately equal to a constant over a wider frequency band as the value of  $C_2$  increases. Therefore, the mutual coupling between the two resonators is designed to be as large as possible to realize a flat  $\text{Im}\{Y_{21}^N\}$ , while its absolute value can be independently adjusted by adjusting  $C_3$  and  $\theta_1$ , as can be seen in Fig. 4.

### III. DESIGN EXAMPLES

To validate the proposed decoupling scheme and its design theory, two examples concerning different antenna coupling mechanisms are presented. In both cases, the coupled antennas are fabricated on an FR4 substrate with relative dielectric constant of 4.4 and thickness of 1.6 mm. The two resonators and their coupling capacitor are integrated into an LTCC device whose relative dielectric constant is 9.2 and loss tangent is 0.002 at the frequency of interest. With an eight-layer vertical structure, the LTCC device is with dimensions of  $3.2 \times 2.5 \times 1.2$  mm<sup>3</sup>. Full-wave EM simulation is performed using Agilent EMPro [24].

#### A. Decoupling Networks for a Symmetric Array

A symmetric 2.45-GHz two-element antenna array and the manufactured LTCC decoupling device will be discussed in this section. The configuration of the entire network, the detailed layout of the LTCC device, and the EM model of the device together with a printed circuit board (PCB) are illustrated in Fig. 6. As can be seen, two coupled monopole antennas separated by distance  $D$  are printed on a  $90$  mm  $\times$   $72$  mm FR4

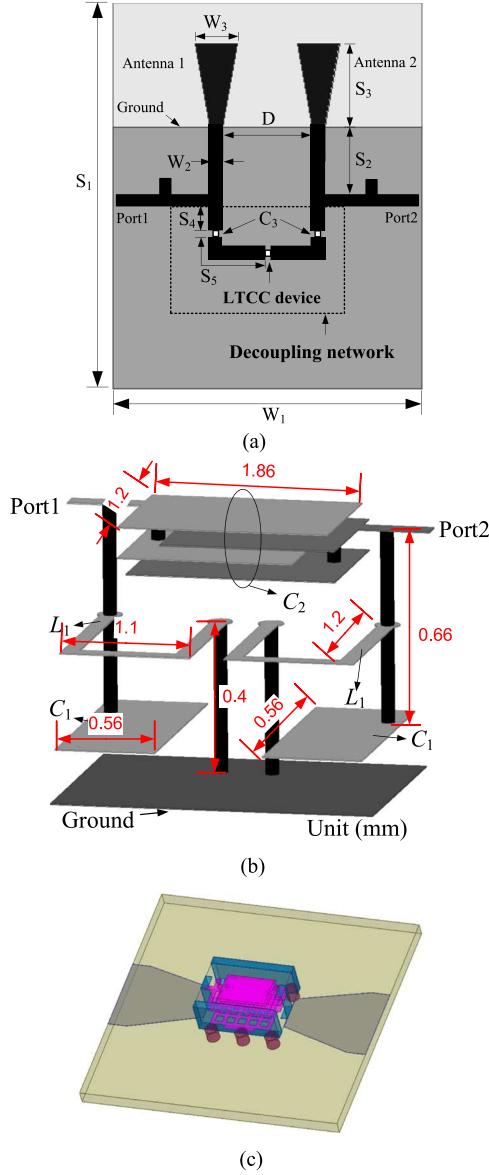
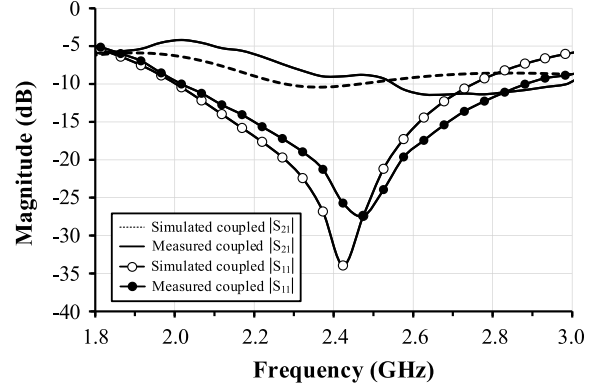


Fig. 6. Configurations of the: (a) symmetric 2.45-GHz testing antenna array, (b) layout of the LTCC device with detail dimensions, and (c) EM model of the LTCC device surface mounted on a PCB.

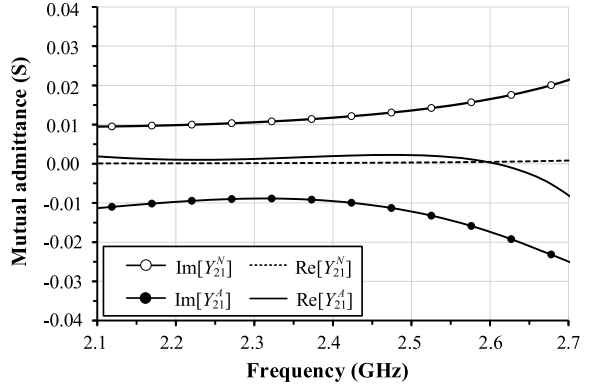
board. The other antenna relevant dimensions are  $W_2 = 3$  mm,  $W_3 = 9.8$  mm, and  $S_3 = 19.4$  mm. A section of transmission line of length  $S_2$  and characteristic impedance of  $Z_0$  is inserted at each antenna port to satisfy (4).

The parameters  $L_1$ ,  $\theta_1$ ,  $C_1$ ,  $C_2$ , and  $C_3$  are designed by following the procedure given in Section II-B. Two open stubs are utilized near ports 1 and 2 for improving the matching bandwidth. With the predesigned LTCC device and proper I/O couplings, different types of coupled antennas working at the 2.45-GHz band can be decoupled with good impedance matching.

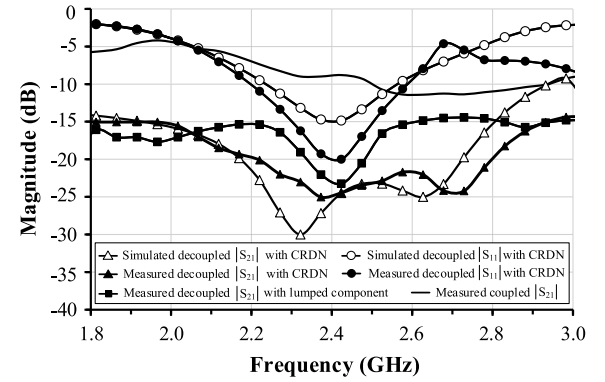
Antenna pairs with  $D = 0.1\lambda_0$  and  $D = 0.2\lambda_0$  are investigated for different coupling circumstances, where  $\lambda_0$  is the free-space wavelength at 2.45 GHz. In the case of array A1 (symmetric,  $D = 0.1\lambda_0$ ), the simulated and measured  $S$ -parameters of the coupled array are given in Fig. 7(a), in which the isolation of about 8 dB of the coupled array in the working frequency



(a)



(b)



(c)

Fig. 7. (a) Simulated and measured  $S$ -parameters of the coupled array A1. (b) Simulated mutual admittances of the antenna array A1 and the decoupling network. (c) Simulated and measured responses of the decoupled array A1.

band is also superimposed. In order to realize  $\text{Re}\{Y_{21}^A\} = 0$  at the resonant frequency, the inserted transmission line has a length of  $S_2 = 19$  mm. The  $\text{Im}\{Y_{21}^N\}$  is designed to be 0.012 to cancel the  $\text{Im}\{Y_{21}^A\}$  that is about  $-0.012$  in the vicinity of resonant frequency, as shown in Fig. 7(b). Due to the compact volume and LTCC fabrication constraints, the mutual coupling  $C_2$  realized in the LTCC device is limited to 6 pF. The other parameters of the decoupling network are designed as follows:  $L_1 = 3.5$  nH,  $C_1 = 1.0$  pF,  $C_3 = 0.9$  pF,  $S_4 = 4$  mm, and  $S_5 = 9.8$  mm, which corresponds to the design parameter  $\theta_1$ .

Fig. 7(c) shows the simulated and measured  $S$ -parameters of the decoupled antennas, as well as the  $|S_{21}|$  of the coupled antennas. It can be seen that the decoupling bandwidth with  $|S_{21}| \leq -20$  dB is about 24% (580 MHz), while the impedance matching bandwidth with  $|S_{11}| \leq -10$  dB is about 17%

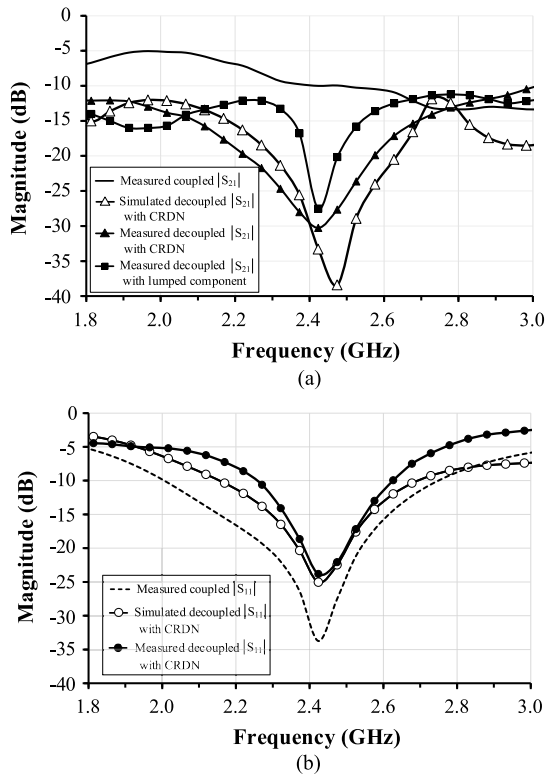


Fig. 8. (a) Simulated and measured isolations of the coupled and decoupled array A2. (b) Simulated and measured reflection coefficients of the coupled and decoupled array A2.

(400 MHz). For comparison, the same antennas are decoupled by a lumped element designed using the procedure given in [8]. It is seen from Fig. 7(c) that the decoupling bandwidth with  $|S_{21}| \leq -20$  dB using a lumped element is about 6% (150 MHz). In the case of array A2 (symmetric,  $D = 0.2\lambda_0$ ), the isolation of the coupled array is about 10 dB in the operating frequency band. In this case,  $S_2 = 16.3$  mm is utilized for realizing  $\text{Re}\{Y_{21}^A\} = 0$  and the corresponding  $\text{Im}\{Y_{21}^A\}$  is about  $-0.008$ . With the same LTCC device, the other circuit parameters of the CRDN are tuned to realize  $\text{Im}\{Y_{21}^N\} = 0.008$  and  $\text{Im}\{Y_{11}^N\} = 0$  in the frequency band of interest, resulting in  $C_3 = 1.8$  pF,  $S_4 = 3.1$  mm, and  $S_5 = 9.2$  mm. Fig. 8 shows the simulated and measured  $S$ -parameters of the decoupled array A2. The decoupling bandwidth with  $|S_{21}| \leq -20$  dB is about 14% (360 MHz), and the impedance matching bandwidth with  $|S_{11}| \leq -10$  dB is about 15% (370 MHz). Similarly, in contrast, the same array decoupled by a lumped element has a decoupling bandwidth of about 3.7% for 20-dB isolation.

### B. Decoupling Networks for Asymmetric Arrays

In order to further demonstrate the effectiveness of the LTCC CRDN device, an asymmetric antenna array with two different types of antennas is the concern of this section. The geometries of the antennas and corresponding CRDN circuit are depicted in Fig. 9. An inverted-F antenna and a monopole antenna are printed on an FR4 substrate with the size of  $120 \text{ mm} \times 120 \text{ mm}$ . The dimensions of the antennas are  $W_2 = 3$  mm,  $W_3 = 9$  mm,  $S_2 = 0.2$  mm,  $S_3 = 7$  mm, and  $S_7 = 18.4$  mm. Similarly, a section of transmission line is introduced according to (4), and  $D = 0.3\lambda_0$  and  $D = 0.4\lambda_0$  cases are investigated in

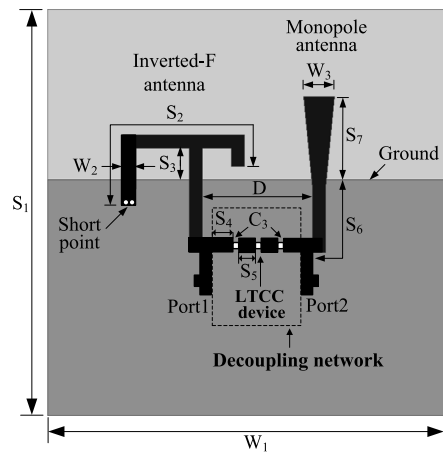


Fig. 9. Configurations of the asymmetric antenna array and LTCC CRDN circuit.

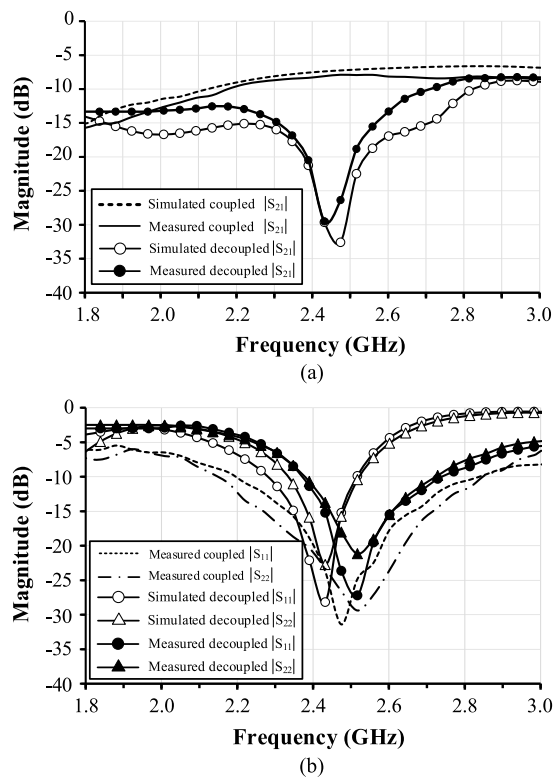


Fig. 10. (a) Simulated and measured isolations of the coupled and decoupled array B1. (b) Simulated and measured reflection responses of the coupled and decoupled array B1.

this example. Also, two open stubs are used for broadening the matching bandwidth.

In the case of array B1 (asymmetric,  $D = 0.3\lambda_0$ ), the isolation of the coupled array is about 7 dB in the operating frequency band. Here,  $S_6 = 16$  mm is used to realize  $\text{Re}\{Y_{21}^A\} = 0$  and  $\text{Im}\{Y_{21}^A\}$  is about  $-0.015$  over a wide frequency range, thus  $\text{Im}\{Y_{21}^N\}$  is designed to be about 0.015 by choosing  $C_3 = 1.2$  pF,  $S_4 = 4.6$  mm, and  $S_5 = 6.2$  mm. The simulated and measured  $S$ -parameters of decoupled array B1 are shown in Fig. 10(a) and (b). It is illustrated that the decoupling bandwidth with  $|S_{21}| \leq -20$  dB is about 11% (280 MHz), while the impedance matching bandwidth with  $|S_{11}| \leq -10$  dB is about 13.5% (330 MHz), and  $|S_{22}| \leq -10$  dB is about 13% (320 MHz).

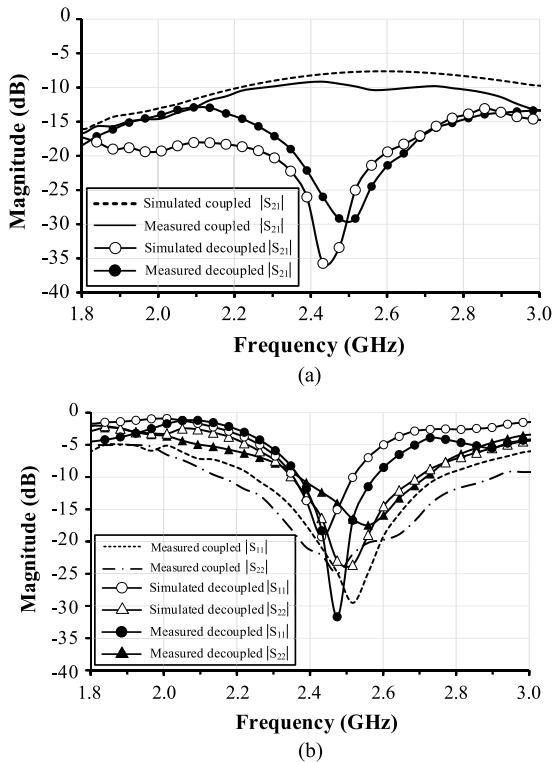


Fig. 11. (a) Simulated and measured isolations of the coupled and decoupled array B2. (b) Simulated and measured reflection coefficients of the coupled and decoupled array B2.

In the case of array B2 (asymmetric,  $D = 0.4\lambda_0$ ), the isolation of the coupled array is about 9.5 dB from 2.4 to 2.48 GHz. Here,  $S_6 = 13$  mm is used for  $\text{Re}\{Y_{21}^A\} = 0$  and  $\text{Im}\{Y_{21}^A\}$  is about  $-0.011$ . Accordingly, the other parameters are  $C_3 = 1.5$  pF,  $S_4 = 3.2$  mm, and  $S_5 = 7.7$  mm. Fig. 11 shows the simulated and measured S-parameters of decoupled array B2. The decoupling bandwidth with  $|S_{21}| \leq -20$  dB is about 12% (290 MHz), while the impedance-matching bandwidth with  $|S_{11}| \leq -10$  dB is about 9% (210 MHz), and  $|S_{22}| \leq -10$  dB is about 14% (350 MHz). The photographs of the antenna arrays along with some samples of the manufactured LTCC CRDN device are shown in Fig. 12.

For all the cases, it is seen that when an LTCC CRDN device is added to a coupled antenna array, the matching bandwidth decreases. The reason for this is that for strongly coupled antennas, one antenna acts as a lossy load for the other one. Thus, it is understandable that the matching bandwidth for the lossier antenna is greater. However, despite the reduced matching bandwidth, the total efficiencies, which are the averaged efficiencies of the two antennas of an array, of the decoupled antenna arrays is significantly improved over the arrays before decoupling. As presented in Fig. 13(a), the measured average total efficiencies of the four coupled arrays A1, A2, B1, and B2 are about 69.4%, 70.3%, 71.6%, and 72.7%, respectively, while the total efficiencies of the four arrays have been improved to 78.2%, 78.5%, 79.7%, and 81.2%, respectively, after decoupling. An obvious enhancement in total efficiency can be achieved when the proposed LTCC CRDN is utilized. The envelope correlation coefficient (ECC), another important figure of merit in assessing a MIMO system, is also obtained using the method in [20] for

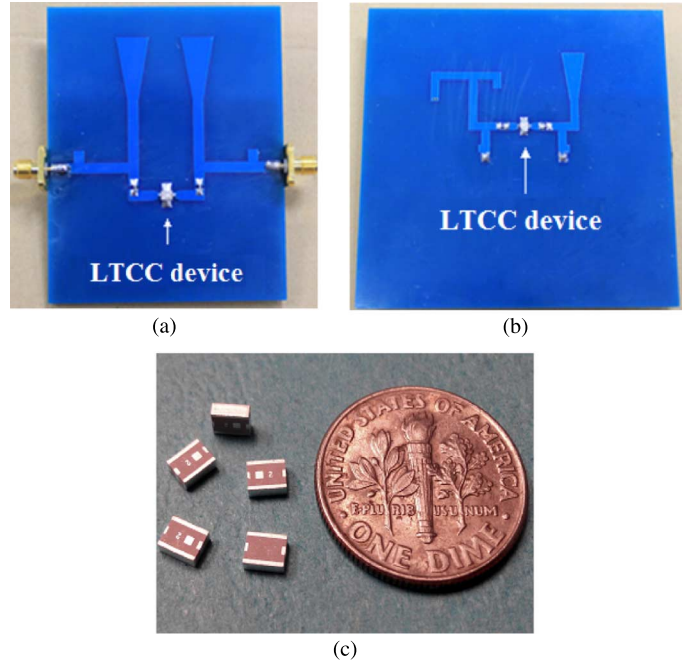


Fig. 12. Photographs of: (a) testing board for symmetric antenna array with an LTCC CRDN device, (b) testing board for asymmetric antenna array with an LTCC CRDN device, and (c) samples of the LTCC CRDN device.

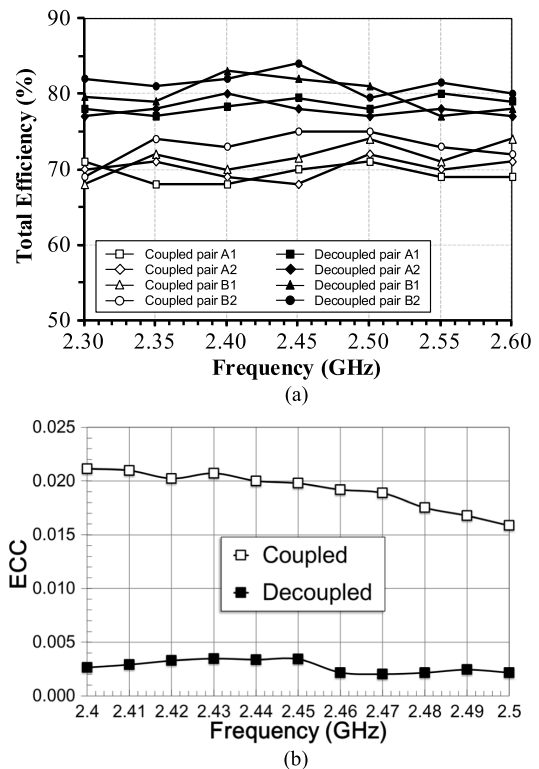


Fig. 13. (a) Total efficiencies of arrays A1, A2, B1, and B2. (b) Calculated ECCs for array B2 and its counterpart without using CRDN.

array B2 and the same antenna array without a CRDN are shown in Fig. 13(b).

#### IV. TRADEOFF ANALYSIS

The prototyped LTCC CRDN device can be used in various decoupling circumstances due to its antenna independence. Furthermore, a tradeoff between the isolation level and decoupling

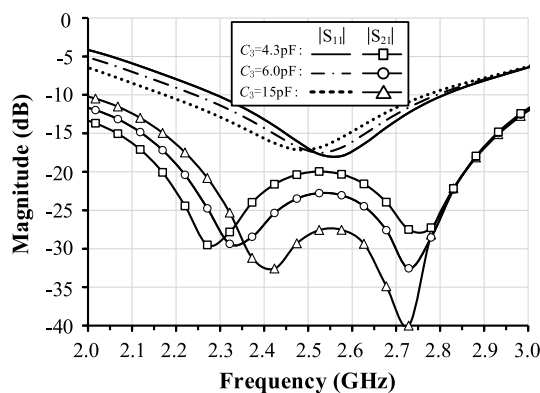


Fig. 14. Tradeoff analysis between the isolation level and decoupling bandwidth with different values of  $C_3$ .

bandwidth can also be realized by adjusting the I/O couplings. A pair of monopole antennas is used here as an illustration of the tradeoff feature. It can be seen from Fig. 14, when the value of  $C_3$  is changed from 4.3 to 15 pF, the decoupling bandwidth for 20-dB isolation is reduced from 680 to 600 MHz, whereas the isolation is improved from 20 to about 28 dB. In all cases, the matching bandwidths remain the same. Therefore, with this antenna-independent LTCC CRDN device and appropriate lumped capacitor  $C_3$ , a tradeoff between the decoupling bandwidth and isolation level can be realized without reconfiguring the CRDN network. This feature allows a mass production of one LTCC device for various applications as long as the frequency band is right.

## V. CONCLUSION

A novel integrated LTCC CRDN has been proposed in this paper. With a consolidated LTCC device for a given frequency band and customized lumped element I/O elements, the proposed decoupling scheme can be applied to various antenna arrays. Taking advantage of the LTCC multilayer technology, the integrated CRDN device can be made in a compact volume. The design theory and guidelines of the proposed device are also given.

To demonstrate the proposed decoupling scheme, four examples working at a 2.45-GHz band of different types of antennas, including symmetric and asymmetric arrays, have been given. All the coupled antenna arrays in this paper have been decoupled using the same LTCC CRDN device, but with different external I/O components. The simulated and measured results verify that good decoupling and matching conditions can be achieved over a wide frequency range as compared to the decoupling solution using a lumped element. A tradeoff between decoupling bandwidths and levels of isolation can also be realized without reconfiguring the integrated device. It can be foreseen that the proposed integrated CRDN device has a great potential for future wireless terminals that are equipped with MIMO antennas.

## REFERENCES

- [1] R. Vaughan and J. B. Anderson, *Channels, Propagation and Antennas for Mobile Communications*. London, U.K.: IEE, 2003.
- [2] M. A. Jensen and J. W. Wallace, "A review of antennas and propagation for MIMO wireless communications," *IEEE Trans. Antennas Propag.*, vol. 52, no. 11, pp. 2810–2824, Nov. 2004.
- [3] J. Weber, C. Volmer, K. Blau, R. Stephan, and M. A. Hein, "Miniaturized antenna arrays using decoupling networks with realistic elements," *IEEE Trans. Microw. Theory Techn.*, vol. 54, no. 6, pp. 2733–2740, Jun. 2006.
- [4] H. Li, Y. Tan, B. K. Lau, Z. Ying, and S. He, "Characteristic mode based tradeoff analysis of antenna-chassis interactions for multiple antenna terminals," *IEEE Trans. Antennas Propag.*, vol. 60, no. 2, pp. 490–502, Feb. 2012.
- [5] L. K. Yeung and Y. E. Wang, "Mode-based beamforming arrays for miniaturized platforms," *IEEE Trans. Microw. Theory Techn.*, vol. 57, no. 1, pp. 45–52, Jan. 2009.
- [6] C. Volmer, J. Weber, R. Stephan, K. Blau, and M. A. Hein, "An eigenanalysis of compact antenna arrays and its application to port decoupling," *IEEE Trans. Antennas Propag.*, vol. 56, no. 2, pp. 360–370, Feb. 2008.
- [7] J. C. Coetzee and Y. Yu, "Port decoupling for small arrays by means of an eigenmode feed network," *IEEE Trans. Antennas Propag.*, vol. 56, no. 6, pp. 1587–1593, Jun. 2008.
- [8] S.-C. Chen, Y.-S. Wang, and S.-J. Chung, "A decoupling technique for increasing the port isolation between two strongly coupled antennas," *IEEE Trans. Antennas Propag.*, vol. 56, no. 12, pp. 3650–3658, Dec. 2008.
- [9] A. Diallo, C. Luxey, P. L. Thuc, R. Staraj, and G. Kossiavas, "Enhanced two-antenna structures for universal mobile telecommunications system diversity terminals," *IET Microw. Antennas Propag.*, vol. 2, pp. 93–101, 2008.
- [10] A. Diallo, C. Luxey, P. L. Thuc, R. Staraj, and G. Kossiavas, "Study and reduction of the mutual coupling between two mobile phone PIFAs operating in the DCS1800 and UMTS bands," *IEEE Trans. Antennas Propag.*, vol. 54, no. 11, pp. 3063–3074, Nov. 2006.
- [11] S.-W. Su, C.-T. Lee, and F.-S. Chang, "Printed MIMO-antenna system using neutralization-line technique for wireless USB-Dongle applications," *IEEE Trans. Antennas Propag.*, vol. 60, no. 2, pp. 456–463, Feb. 2012.
- [12] B. K. Lau and J. B. Andersen, "Simple and efficient decoupling of compact arrays with parasitic scatterers," *IEEE Trans. Antennas Propag.*, vol. 60, no. 2, pp. 464–472, Feb. 2012.
- [13] F. Yang and Y. Rahmat-Sami, "Microstrip antennas integrated with electromagnetic band-gap (EBG) structures: A low mutual coupling design for array applications," *IEEE Trans. Antennas Propag.*, vol. 51, no. 10, pp. 2936–2946, Oct. 2003.
- [14] L. Yang, M. Fan, F. Chen, J. She, and Z. Feng, "A novel compact electromagnetic-bandgap (EBG) structure and its applications for microwave circuits," *IEEE Trans. Microw. Theory Techn.*, vol. 53, no. 1, pp. 183–190, Jan. 2005.
- [15] K. Payandehjoo and R. Abhari, "Employing EBG structures in multi-antenna systems for improving isolation and diversity gain," *IEEE Antennas Wireless Propag. Lett.*, vol. 8, pp. 1162–1165, 2009.
- [16] C. Y. Chiu, C. H. Cheng, R. D. Murch, and C. R. Rowell, "Reduction of mutual coupling between closely-packed antenna element," *IEEE Trans. Antennas Propag.*, vol. 55, no. 6, pp. 1732–1738, Jun. 2007.
- [17] Y. Chung, S.-S. Jeon, D. Ahn, J.-I. Choi, and T. Itoh, "High isolation dual-polarized patch antenna using integrated defected ground structure," *IEEE Microw. Wireless Compon. Lett.*, vol. 14, no. 1, pp. 4–6, Jan. 2004.
- [18] L. Zhao, L. K. Yeung, and K.-L. Wu, "A novel second-order decoupling network for two-element compact antenna arrays," in *Proc. Asia-Pacific Microw. Conf.*, Dec. 2012, pp. 1172–1174.
- [19] L. Zhao and K.-L. Wu, "A broadband coupled resonator decoupling network for a three-element compact array," in *IEEE MTT-S Int. Microw. Symp. Dig.*, Jun. 2013.
- [20] L. Zhao, L. K. Yeung, and K.-L. Wu, "A coupled resonator decoupling network for two-element compact antenna arrays in mobile terminals," *IEEE Trans. Antennas Propag.*, vol. 62, no. 5, pp. 2767–2776, May 2014.
- [21] L. Zhao, K.-W. Qian, and K.-L. Wu, "A cascaded coupled resonator decoupling network for mitigating interference between two radios in adjacent frequency bands," *IEEE Trans. Microw. Theory Techn.*, vol. 62, no. 11, pp. 2680–2688, Nov. 2014.
- [22] L. K. Yeung and K.-L. Wu, "A compact second-order LTCC band-pass filter with two finite transmission zeros," *IEEE Trans. Microw. Theory Techn.*, vol. 51, no. 2, pp. 337–341, Feb. 2003.
- [23] L. K. Yeung, K.-L. Wu, and Y. E. Wang, "Low-temperature cofired ceramic LC filters for RF applications," *IEEE Microw. Mag.*, vol. 9, no. 5, pp. 118–128, Oct. 2008.
- [24] EMPro 3D EM Simulation Software. ver. 2012.09, Agilent Technol., Santa Clara, CA, USA, 2012.



**Kewei Qian** was born in Chongqing, China, in 1981. He received the M.Eng. and Ph.D. degrees from the University of Electronic Science and Technology of China, Chengdu, Sichuan, China, in 2006 and 2012, respectively.

From March 2013 to May 2014, he was with the Department of Electronic Engineering, The Chinese University of Hong Kong, Shatin, NT, Hong Kong, where he was involved in various low-temperature co-fired ceramic (LTCC) multichip-module (MCM) designs and antennas for next-generation mobile communication systems. He is currently an Associate Professor with the University of Electronic Science and Technology of China. His current research interests include design and application of microwave and millimeter wave circuits and systems.



**Luyu Zhao** (S'09–M'14) was born in Xi'an, China, in 1984. He received the B.Eng. degree from Xidian University, Xi'an, China, in 2007, and the Ph.D. degree from The Chinese University of Hong Kong, Shatin, Hong Kong, in 2014.

He is currently a Postdoctoral Fellow with The Chinese University of Hong Kong, Shatin, NT, Hong Kong. From 2007 to 2009, he was with the National Key Laboratory of Antennas and Microwave Technology, Xidian University, as a Research Assistant, where he was involved in software and hardware development of RF identification (RFID) technologies. His current research interests include design and applications of multiple antenna systems for next-generation mobile communication systems, as well as innovative passive RF and microwave components, circuits, and systems.

Mr. Zhao was the recipient of the Best Student Paper Award of the 2013 IEEE 14th HK AP/MTT Postgraduate Conference.



**Ke-Li Wu** (M'90–SM'96–F'11) received the B.S. and M.Eng. degrees from the Nanjing University of Science and Technology, Nanjing, China, in 1982 and 1985, respectively, and the Ph.D. degree from Laval University, Quebec, QC, Canada, in 1989.

From 1989 to 1993, he was with the Communications Research Laboratory, McMaster University, as a Research Engineer and a Group Manager. In March 1993, he joined the Corporate Research and Development Division, COM DEV International, where he was a Principal Member of Technical Staff. Since October 1999, he has been with The Chinese University of Hong Kong, Shatin, NT, Hong Kong, where he is a Professor and the Director of the Radiofrequency Radiation Research Laboratory (R3L). His current research interests include partial-element equivalent-circuit (PEEC) and physics-based model-order reduction for electromagnetic (EM) modeling of high-speed circuits, RF and microwave passive circuits and systems, synthesis theory and computer-aided tuning of microwave filters, antennas for wireless terminals, LTCC-based multichip modules (MCMs), and RF identification (RFID) technologies.

Prof. Wu is a member of the IEEE MTT-8 Subcommittee (Filters and Passive Components). He also serves as a Technical Program Committee (TPC) member for many prestigious international conferences including the IEEE Microwave Theory and Techniques Society (IEEE MTT-S) International Microwave Symposium (IMS). He was an associate editor for the IEEE TRANSACTIONS ON MICROWAVE THEORY AND TECHNIQUES from 2006 to 2009. He was the recipient of the 1998 COM DEV Achievement Award and the Asia-Pacific Microwave Conference Prize in 2008 and 2012, respectively.